

1 Generation of autogenic knickpoints in laboratory landscape  
2 experiments evolving under constant forcing.

3

4 **Léopold de Lavaissière<sup>1</sup>, Stéphane Bonnet<sup>1</sup>, Anne Guyez<sup>1</sup>, and Philippe Davy<sup>2</sup>**

5 <sup>1</sup> *GET, Université de Toulouse, CNRS, IRD, UPS(Toulouse), France,*

6 <sup>2</sup> *Univ Rennes, CNRS, Géosciences Rennes - UMR 6118, 35000 Rennes, France,*

7 Correspondence to: Stéphane Bonnet (stephane.bonnet@get.omp.eu)

8

9 **ABSTRACT**

10 **The upstream propagation of knickpoints in river longitudinal profiles is commonly assumed to**  
11 **be related to discrete changes in tectonics, climate or base-level. However, the recognition that**  
12 **some knickpoints may form autogenically, independent of any external perturbation, may**  
13 **challenge these assumptions. We investigate here the genesis and dynamics of such autogenic**  
14 **knickpoints in laboratory experiments at the drainage basin scale, where landscapes evolved in**  
15 **response to constant rates of base-level fall and precipitation. Despite these constant forcings, we**  
16 **observe that knickpoints regularly initiate in rivers at the catchments' outlet throughout the**  
17 **duration of experiments. The upstream knickpoint propagation rate does not decrease**  
18 **monotonically in relationship with the decrease of drainage area, as predicted by stream-power**  
19 **based models, instead the propagation rate first increases until the mid-part of catchments before**  
20 **decreasing. To investigate the dynamics of the knickpoints, we calculated hydraulic information**  
21 **(water depth, river width, discharge and shear stress) using a hydrodynamic model. We show that**  
22 **knickpoint initiation at the outlet coincides with a fairly abrupt river narrowing entailing an**  
23 **increase in their shear stress. Then, once knickpoints have propagated upward, rivers widen**  
24 **causing a decrease in shear stress and incision rate, and making the river incision less than the**  
25 **base-level fall rate. This creates an unstable situation which drives the formation of a new**

26 **knickpoint. The experiments suggest a new autocyclic model of knickpoint generation controlled**  
27 **by river width dynamics independent of variations in climate or tectonics. This questions an**  
28 **interpretation of landscape records focusing only on climate and tectonic changes without**  
29 **considering autogenic processes.**

## 30 **1 Introduction**

31 Knickpoints are discrete zones of steepened bed gradient that are commonly observed in river  
32 longitudinal profiles. Although they occasionally occur due to changes in bedrock properties (e.g. Duvall  
33 et al., 2004), in many cases they are dynamic features that propagate upstream along drainage networks  
34 (Whipple and Tucker, 1999; Kirby and Whipple, 2012; Whittaker and Boulton, 2012). In this latter case,  
35 they are commonly considered as formed in response to variations in external forcing such as uplift rate,  
36 sea level or climate (e.g. Crosby and Whipple 2006; Berlin and Anderson, 2007; Kirby and Whipple,  
37 2012; Whittaker and Boulton, 2012; Mitchell and Yanites, 2019) which opens the possibility of using  
38 knickpoints in landscapes to identify such changes. Several studies pointed out, however, that some  
39 knickpoints could be autogenic, that is to say internally-generated without any variation in boundary  
40 conditions (e.g. Hasbargen and Paola, 2000, 2003; Finnegan and Dietrich, 2011). Understanding how  
41 knickpoints can form autogenically is therefore crucial for interpreting changes in external forcing from  
42 knickpoint occurrence in landscapes. Most observations of autogenic knickpoints formation come from  
43 experimental modelling (see for example Paola et al., 2009) their initiation being attributed to  
44 amplification of local instabilities in flume (Scheingross et al., 2019) and drainage basin scale  
45 (Hasbargen and Paola, 2000), experiments. In these latter experiments for example, successive  
46 knickpoints initiated despite constant external forcing (base-level fall and precipitation) throughout the  
47 duration of the runs, even when landscapes were at steady-state on average in terms of sediment flux.  
48 Internal processes may also complexify the propagation of knickpoints as shown in the flume  
49 experiments of Cantelli and Muto (2014) and Grimaud et al. (2016) where a single discrete event of  
50 base-level drop resulted in the propagation of multiple waves of knickpoints.

51 .

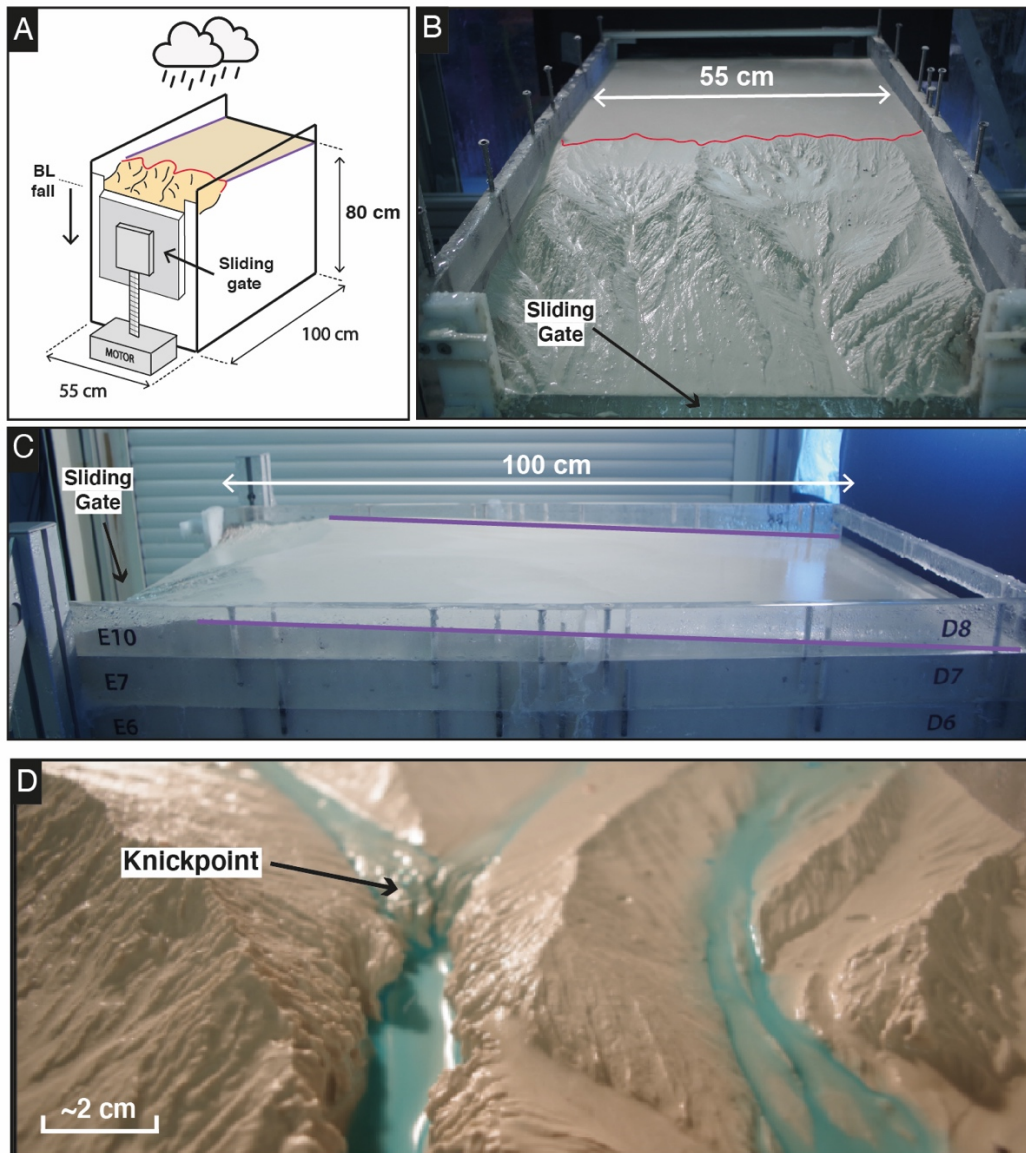
52 In this work, we consider the generation and dynamics of autogenic knickpoints in laboratory-scale  
53 drainage basins experiments forced by constant rate of base-level fall and steady precipitation. Such  
54 landscape experiments have been used successfully to explore how tectonics and climate impact erosion  
55 processes and the evolution of topography under controlled conditions (e.g. Hasbargen and Paola, 2000;  
56 Bonnet and Crave, 2003; Lague et al., 2003; Turowski et al., 2006; Bonnet, 2009; Singh et al., 2015;  
57 Sweeney et al., 2015; Moussirou and Bonnet, 2018). This approach allows for the observation of  
58 complex dynamics that are sometimes difficult to simulate numerically and sheds new light on the way  
59 natural landforms may evolve. Landscape experiments capture the tree-like structure of drainage  
60 networks, the supply of eroded material from hillslopes, and especially their fluctuations, which is a  
61 natural complexity that is not reproduced in flume experiments, for example. The experiments presented  
62 here have been performed using a new setup specifically designed to investigate the evolution of a large,  
63 meter-long, single drainage basin under controlled forcing condition. In previous similar catchment-  
64 scale experiments (Hasbargen and Paola, 2000, 2003; Bigi et al., 2006; Rohais et al., 2012) the outlet  
65 location was pinned to a narrow motor-controlled gate used to simulate base-level fall and which also  
66 set the river width at the outlet. A specificity of our setup here is to use a large gate instead of a narrow  
67 one, allowing experimental rivers to freely evolve downstream, with no constraints on their width. We  
68 report here results from experiments where successive knickpoints initiate near the outlet autogenically  
69 and propagate within drainage basins. The experiments show a new model of autogenic knickpoint  
70 initiation and propagation driven by downstream river width dynamics.

71

## 72 **2 Methods**

73 We present here results from 3 experiments, BL05, BL10 and BL15, performed with different rates of  
74 base level fall, of respectively 5, 10 and 15 mm h<sup>-1</sup> (Table 1). The facility is a box with dimensions 100  
75 x 55 cm filled with silica paste (Fig. 1; see also Fig. S1 in the Supplemental Material). At its front side,  
76 a sliding gate, 41 cm-wide, drops down at constant rate, acting as the base level. The initial surface  
77 consists on a plane with a counterslope of ~3°, opposite to the base level-side (Fig. 1C). During a run,  
78 runoff-induced erosion occurs in response to steady base level fall and rainfall (mean rainfall rate is 95

79 mm h<sup>-1</sup> with a spatial coefficient of variation (standard deviation/mean) of 35%). Incision initiates at  
80 some point along the base level and propagates upstream until complete dissection of the initial surface.  
81 Note that the counterslope of the initial surface allows separating the rainfall flux between the base level  
82 and the opposite side of the device, creating a water divide (Fig. 1B).



83

84 **Figure 1.** Experimental setup. Purple and red lines show respectively the counter-slope of the initial  
85 topography and the main water divide. (A) Sketch of the erosion box with the sliding gate, 41 cm wide,  
86 used to drop down the base level (BL). (B), (C) Front and side photographs (experiments BL10 at 525  
87 min and BL15 at 185 min). (D) Photograph of a typical knickpoint studied here.

88

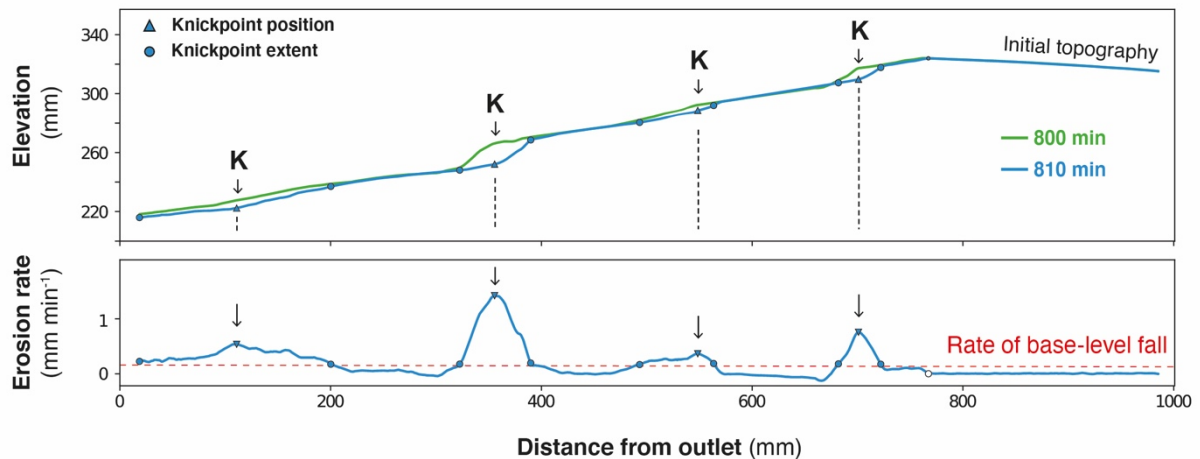
89 **Table 1. Parameters of experiments**

Experiments	Base Level Fall (mm/h)	Precipitation Rate (mm/h)	Duration Time (min)	Mean Divide Retreat Rate (mm/h)	nDDVmax*	Mean Knickpoint Retreat Rate (mm/h)
BL15	15	95	1065	66.3	0.52	183.6 ± 93.8
BL10	10	95	1200	55.7	0.57	164.8 ± 74.8
BL05	5	95	1455	25	0.54	73.1 ± 50

90 \*nDDVmax : normalized distance of maximum knickpoint velocity

91 Experiments were stopped every 5 min to digitize the topography using a laser sheet and to construct  
 92 Digital Elevation Models (DEMs) with a pixel size of 1 mm<sup>2</sup>. Longitudinal profiles and knickpoints  
 93 were extracted with a semi-automatic procedure that had to be developed to process the ~200 DEMs per  
 94 experiment. For this purpose, we first extracted longitudinal profiles by finding the lowest elevation on  
 95 successive rows (lines oriented parallel to the sliding gate) of each DEM within a 20 cm-wide swath  
 96 perpendicular to the sliding gate that included the main river (the one with the largest catchment for each  
 97 experiment). Then the lowest elevation found in our search was plotted against distance down the long  
 98 axis of the box. This procedure has already been applied by Baynes et al. (2018) and Tofelde et al.  
 99 (2019). It may result in a slight overestimation in channel slope because it does not consider the obliquity  
 100 of channels within the box in the distance calculation nor their sinuosity. However, these effects are of  
 101 minor influence here, because most channels are straight and roughly parallel to the long side of the box.  
 102 In a second step, we computed the erosion rates by considering elevation difference between each  
 103 successive pairs of longitudinal profiles and we identified knickpoints as peaks in erosion rates with  
 104 values above the steady erosion amount defined by the rate of base-level fall (Fig. 2). We verified  
 105 manually that this procedure defines knickpoints correctly by checking the computed positions on  
 106 longitudinal profiles. We investigated in particular if the procedure is robust with respect to the time  
 107 interval between successive profiles. We found that the record interval of 5 minutes is too small to  
 108 produce well-defined erosional peaks, which lead us to identify knickpoint positions from a time-interval  
 109 of 10 minutes. Then, we built a first catalogue of knickpoints positions at different times from which we  
 110 manually extract the successive positions of each individual knickpoint. We complemented the database  
 111 by computing incremental retreat rates of knickpoints from their successive positions.

112



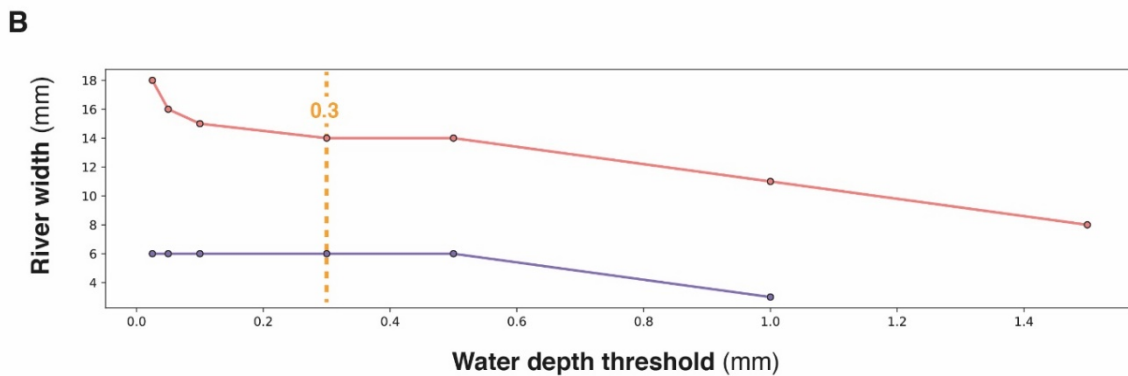
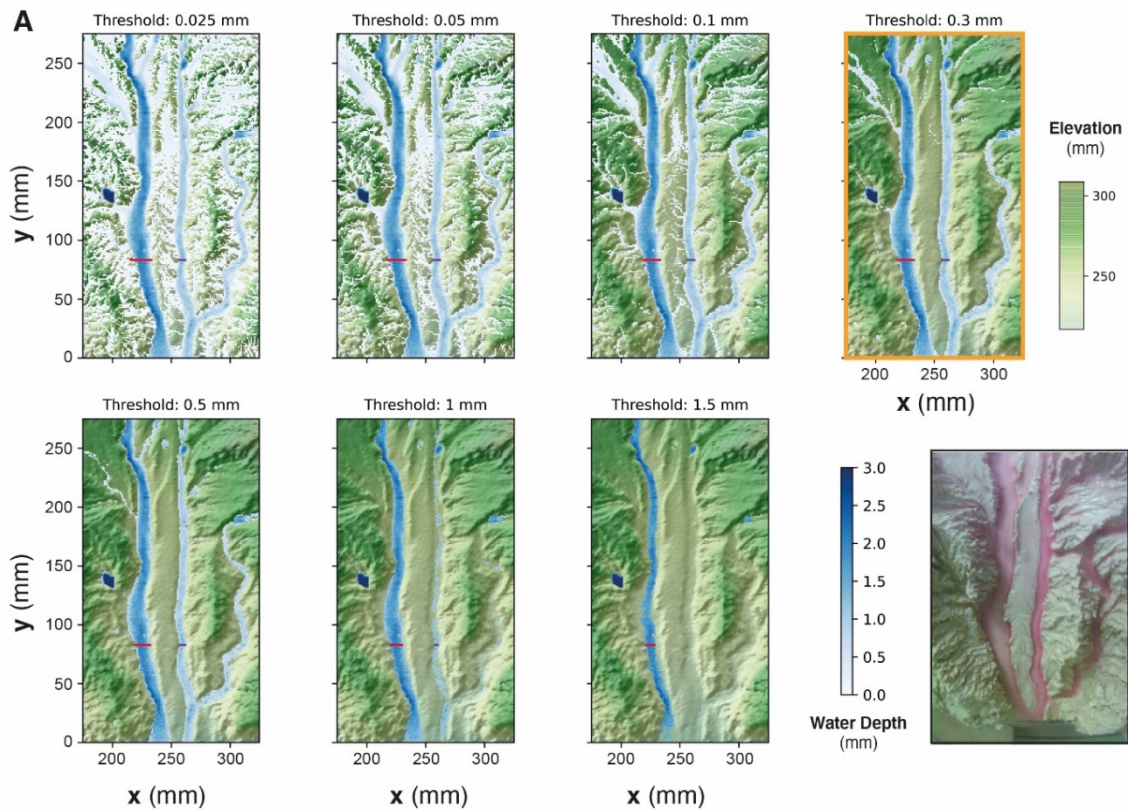
113

114 **Figure 2.** Graph showing two successive longitudinal profiles of experiment BL10 taken at 10 min  
 115 interval (top) and corresponding erosion rate profile (bottom). Triangles illustrate the position of  
 116 erosional peaks taken as knickpoint position (black arrows). Red dashed line shows the rate of base-  
 117 level fall.

118

119 DEMs were also used to compute hydraulic information (water depth, river width, discharge and shear  
 120 stress) using the Floodos hydrodynamic model of Davy et al. (2017; see also Baynes et al. (2018,  
 121 2020) for previous use of Floodos for analyzing laboratory experiments). Floodos is a precipitation-based  
 122 model that calculates the 2D shallow water equations (SWE) without inertia terms, from the routing of  
 123 elementary water volumes on top of topography. We ran Floodos on successive DEMs of experiments  
 124 by inputting spatial distribution of precipitation, then generating several output raster products at the  
 125 pixel size, including water depth, unit discharge and bed shear stress that were then used for  
 126 computation of hydrologic parameters (river width, specific discharge and shear stress). The solution  
 127 of the SWE depends on the friction coefficient (C) that depends on water viscosity only for laminar  
 128 flow; its theoretical value is  $\sim 2.5 \times 10^6 \text{ m}^{-1} \text{ s}^{-1}$  at  $10^\circ\text{C}$  (Baynes et al., 2018). To ensure that Floodos  
 129 outputs (e.g. water depth raster maps) calculated using this value are consistent with actual experiment  
 130 hydraulic conditions, we injected dye in the rainfall water during a run to catch the actual extent of  
 131 water flow and make rivers visible. A visual comparison with Floodos results shows a good match  
 132 between model outputs and experimental results (Fig. S2), which validates the numerical method and

133 the expected theoretical friction coefficient  $C$  (Baynes et al., 2018). Given the difficulty to measure the  
 134 mm-scale water depth without perturbing the flow, river widths were extracted from Floodos DEM  
 135 outputs by thresholding the water depth maps considering that river banks correspond to sharp  
 136 variations in water depth. The water depth threshold was estimated by trial and error by comparing the  
 137 the rivers extracted from the calculation with direct observations on experiments where rainwater was  
 138 colored by red dye (Fig. 3). A good visual agreement was obtained for a threshold value of the water  
 139 depth between 0.1 and 0.5 mm, and a mid-value of 0.3 mm was then used for determining river  
 140 widths.  
 141



142

143 **Figure 3.** *Impact of water depth threshold used to delineate river boundaries on estimated river widths.*  
144 *A. Map views of water depths (blue colors) superimposed to DEM, for water depth threshold values*  
145 *between 0.025 and 1.5 mm. Red and purple lines show corresponding river widths for two rivers. Photo*  
146 *on the bottom right shows the active river width during the corresponding experimental run (“control*  
147 *run”), viewed by injecting red dye in the water used to generate the artificial rainfall. B. Corresponding*  
148 *local river widths for the two sections shown by red and purple lines. A threshold value of between 0.1*  
149 *and 0.5 mm shows a good similarity between rivers on water depth map and the control run. Here, a*  
150 *mid-value of 0.3 mm has been chosen for computing river widths.*

151

## 152 **3 Results**

### 153 **3.1 Dynamics of knickpoints retreat**

154 In each experiment, base level fall induces the growth of drainage networks by headward erosion and  
155 the progressive migration of a main water divide (Fig. 4). The migration rate of the divide is constant in  
156 each experiment (Fig. 5 and Table 1), and this value increases from 25 to 66 mm h<sup>-1</sup> with prescribed rate  
157 of base level fall of 5 to 15 mm h<sup>-1</sup>. The successive longitudinal profiles of the main river investigated  
158 in each experiment (Fig. 6) illustrate the growth of rivers as they propagate within the box. These profiles  
159 show alternations of segments with low and high slopes, the latter defining knickpoints. Knickpoints  
160 regularly initiate at the outlet throughout the duration of the runs in all experiments and propagate  
161 upward until they reach and merge with the divide, some profiles showing even several knickpoints that  
162 retreat simultaneously (Fig. 6). A characteristic of these knickpoints highlighted in Figure 7 (see also  
163 Fig. 6) is that they generally initiate downstream with a gentle slope and gradually steepen as they  
164 migrate upstream. Their maximum slope is generally reached when they have propagated to the central  
165 part of the profiles (see below). Then the slope is maintained or slightly decreases during their retreat in  
166 the upper segment of the profiles.

167 The mean retreat velocity of knickpoints varies between experiments from 73 ± 50 to 183 ± 94 mm h<sup>-1</sup>  
168 (Table 1) and increases as a function of the rate of base-level fall. Data suggest a non-linear relationship



169 between base-level fall rate and mean retreat velocity of knickpoints, however complementary  
170 experiments would be necessary to constraint this dependency. To investigate the propagation of the  
171 knickpoints, we built space-time diagrams (Fig. 8) by plotting the successive alongstream position of  
172 each knickpoint over experimental runtime, as well as the position of the water divide in the box as  
173 already reported in Figure 5. To compare the dynamics of knickpoints within an experiment regardless  
174 of the stage of water divide retreat into the box, the position of knickpoints (distance to outlet,  $D$ ) has  
175 been normalized to the position of the divide, hereafter referred to as normalized distance to divide  
176 ( $nDD$ ;  $nDD=0$  at outlet and  $nDD=1$  at the divide; Fig. 4). Lines of isovalue of  $nDD$  considering an  
177 increment of 0.1 are also shown in the space-time diagrams (Fig. 8). To a first order, the trajectories of  
178 each knickpoint are very comparable within an experiment regardless the stage of retreat of the water  
179 divide and the size of the catchment. Visually for example, in the space-time diagrams there is no  
180 systematic variation in the general slope of the successive knickpoint trajectories over time, as the rivers  
181 expand, that would indicate a change in mean knickpoint velocity in relation to the change in the river  
182 length and catchment size. In detail, an inflection of trajectories is visible for many knickpoints when  
183 they are close to the divide, for  $nDD > \sim 0.8$  (Figure 8), which indicates that they slow down as they  
184 approach the divide. The opposite is observed for some knickpoints when they are close to the outlet,  
185 for  $nDD < \sim 0.2 / 0.3$ , with some trajectories suggesting, on the contrary, an acceleration after their  
186 initiation (Fig. 8; see also Fig. 7). These qualitative interpretations are supported by the detail analysis  
187 of retreat velocity data shown in Figure 9. For each experiment, we show in Figure 9A the stack of  
188 successive retreat velocities of each individual knickpoint according to distance  $nDD$ . These data show  
189 that the range of knickpoint retreat rates depends on the rate of base-level fall. Moreover, the envelopes  
190 draw a bell-shaped distribution for each experiment, which suggests that retreat velocities are maximum  
191 when knickpoints are located at a mid-distance between the outlet and the divide, for central values of  
192  $nDD$ , between 0.4 and 0.6. This is supported by summary statistics of retreat velocities at 0.1 intervals  
193 of  $nDD$  considering all knickpoints in each experiment (Fig. 9B). Both the mean and median values  
194 show higher rates of upstream propagation when knickpoints are in the central section of rivers in the  
195 three experiments, and conversely lower rates near the outlet ( $nDD < 0.2 / 0.3$ ) where they initiate and  
196 start to propagate and near the divide ( $nDD > 0.8$ ), as suggested by trajectories shown in Figure 8. To

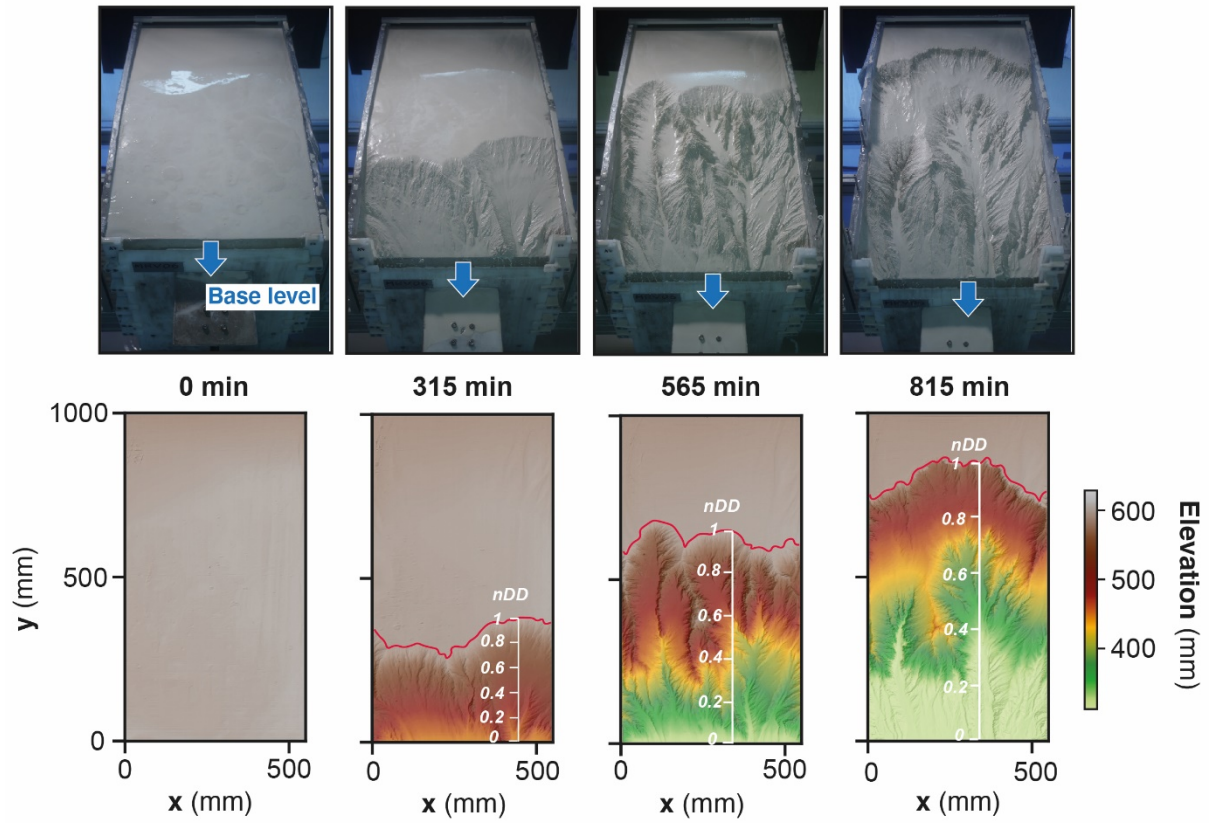
197 further characterize this trend, we determined the position of maximum knickpoint velocity on  
198 longitudinal profiles, hereafter  $nDD_{V_{max}}$ , from a second order polynomial fit (Fig. 9C).  $nDD_{V_{max}}$  values  
199 are very similar between experiments (0.52, 0.57 and 0.54: Table 1). They separate positive to negative  
200 trends of knickpoint velocities versus normalized distance as also illustrated in Figure S4 (see  
201 Supplemental Material). Data from the three experiments indicate that after their initiation near the  
202 outlet, knickpoints first speed up with a maximum in the central part of the catchments before  
203 decelerating near the divide. It is worth noting that this specific trend of knickpoint retreat rates is  
204 observed regardless of the experiment stages and thus whatever the position of the divide in the box.  
205 This applies both to rivers in the early stages of experiments evolution, i.e. when they are small as well  
206 as for very large rivers at the end of experiments.

207

208

209

210



211

212 **Figure 4.** Photos (top row) and corresponding DEMs (bottom row) of experiment BL15 at four runtimes.

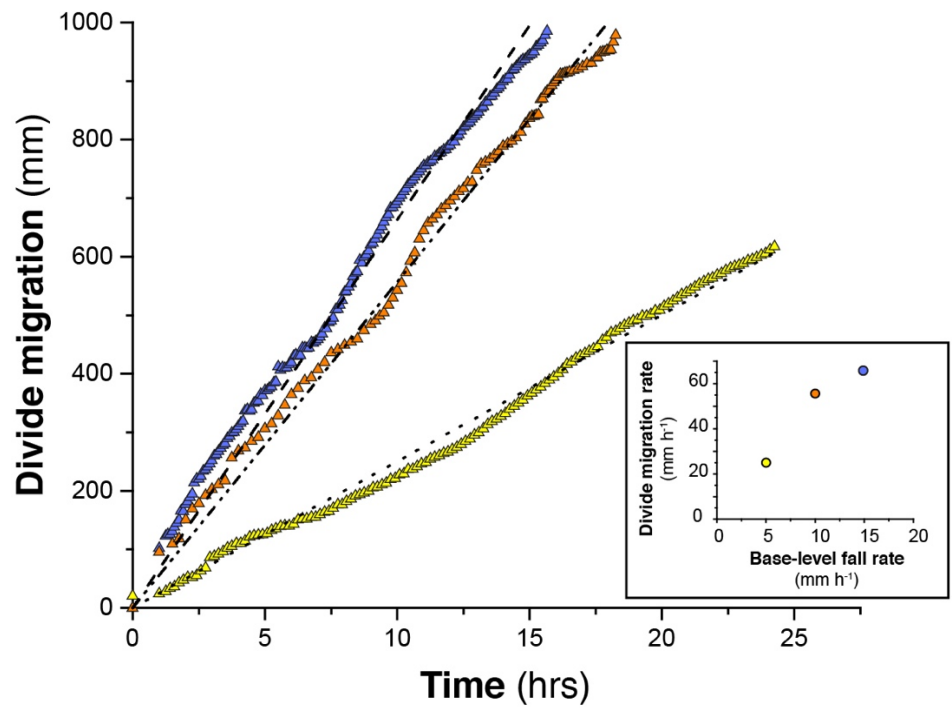
213 Note the propagation of the divide (red line) through the erosion box and the drop of the sliding gate

214 used for falling base-level (blue arrows). The normalized distance to divide (nDD, see text) used to

215 follow the position of knickpoints during runs is shown superimposed to DEMs.

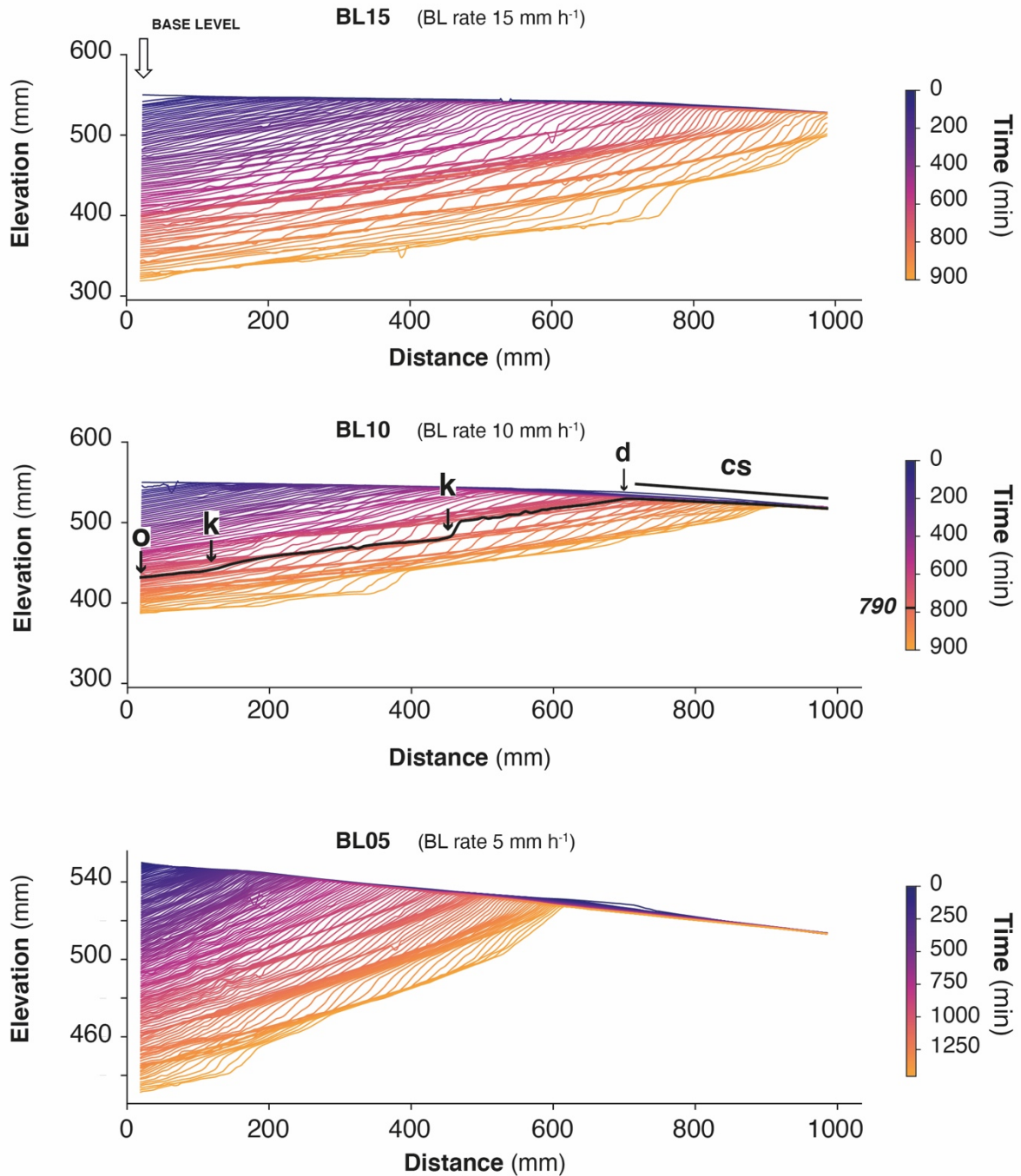
216

- ▲ **BL15**  
- - -  $y = 66.3 x$   $R^2 = 0.99$
- ▲ **BL10**  
- - -  $y = 55.7 x$   $R^2 = 0.99$
- ▲ **BL05**  
- - -  $y = 25.0 x$   $R^2 = 0.99$



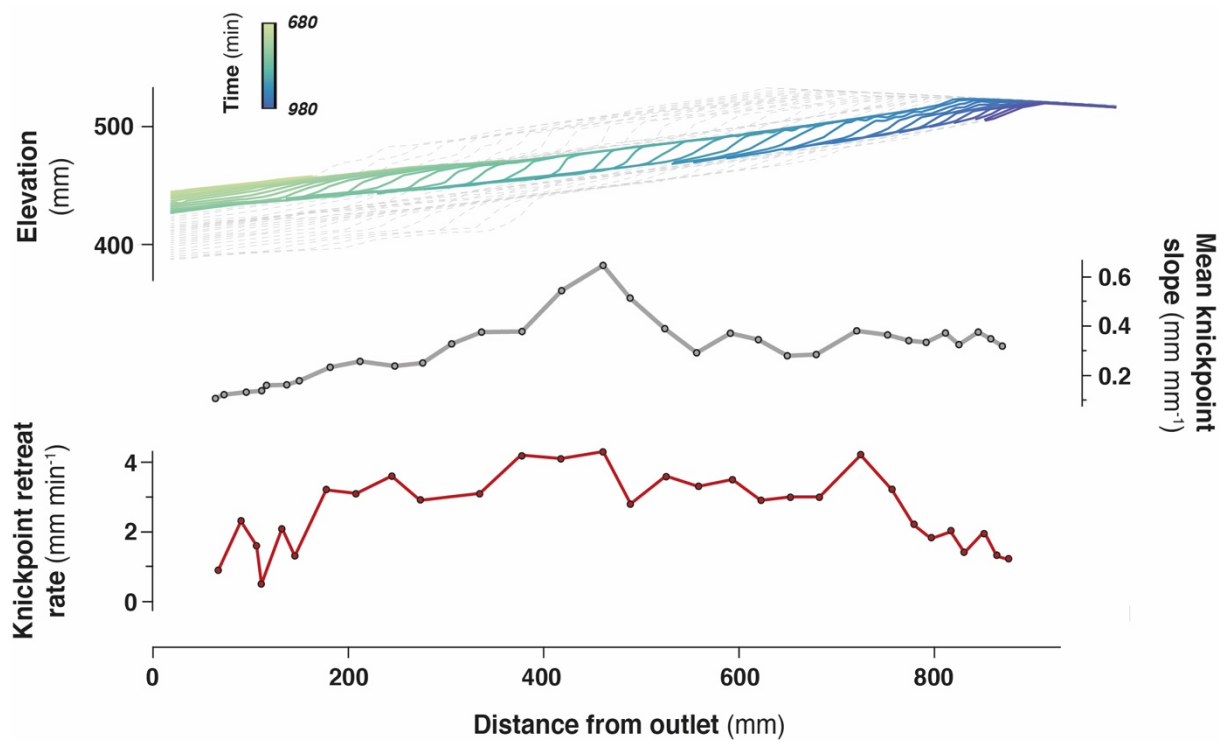
217

218 **Figure 5.** Evolution of the water divide position within the erosion box for the three experiments. The  
 219 inset figure (Bottom right) shows the relation between the divide migration rate in the three experiments  
 220 and their related base-level fall rate.



221

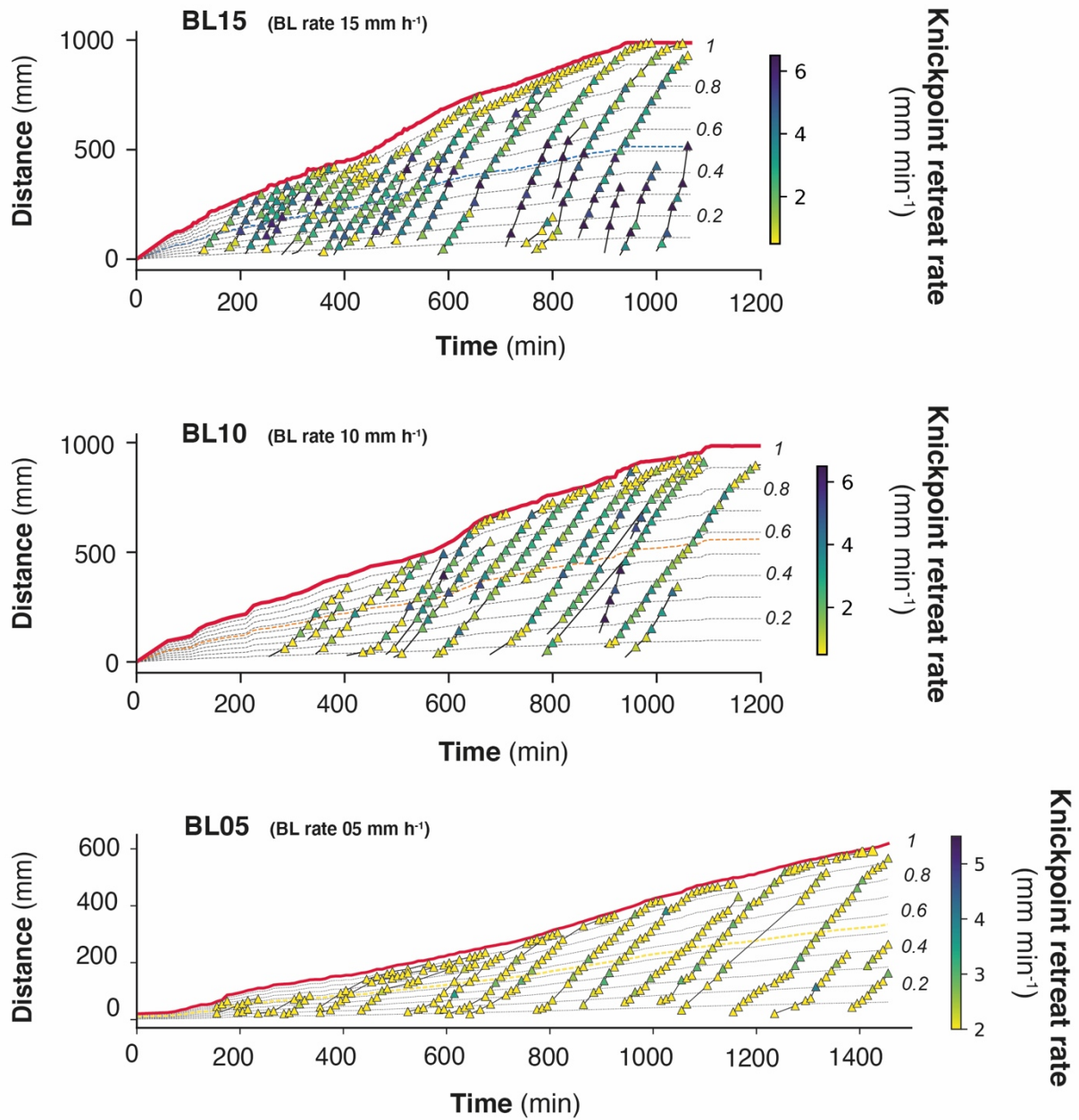
222 **Figure 6.** Successive river longitudinal profiles of experiments, shown here every 10 min. Each  
 223 longitudinal profile is colored according to experimental runtime. The sliding gate used to drop the base  
 224 level is to the left. Note the initial counterslope (cs). Black thick line on BL10 is the longitudinal profile  
 225 at  $t=790$  min, illustrating the outlet (o), knickpoints (k), and water divide (d). Note the change of scale  
 226 for experiment BL05.



227

228 **Figure 7.** Retreat of an individual knickpoint from experiment BL10 (see also Fig. 6) showing its  
 229 initiation with a gentle slope which subsequently steepen as it migrates upstream (see also Fig. S3 in  
 230 the Supplemental Material). Its maximum slope is reached at mid-distance between the outlet and the  
 231 divide. Its lowest retreat rates are observed downstream near the outlet and upstream near the divide.

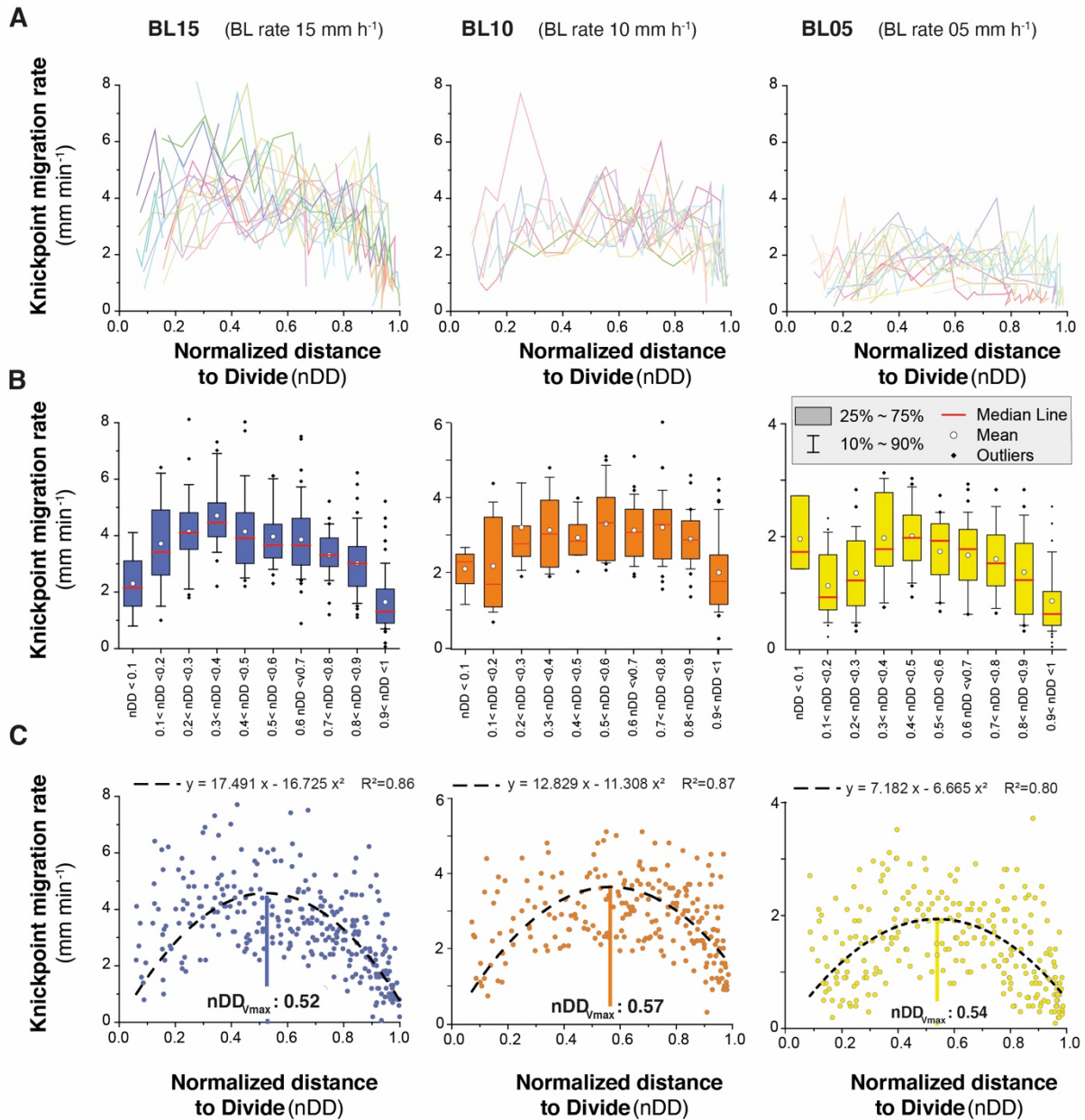
232



233

234 **Figure 8.** Space-time diagrams showing the propagation of the water divide (red line) and successive  
 235 trajectories of knickpoints (triangles). Symbols color shows instant (10 min) knickpoints retreat rate.  
 236 Thin black dashed lines show the normalized distances to divide ( $nDD$ ). Thin colored dashed lines show  
 237  $nDD_{V_{max}}$ , the normalized distance where the highest rate of retreat velocity is deduced from the analysis  
 238 (see text and Figure 9C). Note the change of scale and color bar for experiment BL10.

239



240

241 **Figure 9.** (A) Knickpoint retreat rates according to the normalized distances to divide (nDD) for each  
 242 knickpoint of experiments. Each color line corresponds to an individual knickpoint of the space-time  
 243 diagram in Fig. 8. Note that the scale on the y-axis is the same for all graphs. (B) Summary statistics of  
 244 retreat rates for nDD intervals of 0.1. Note the change in scale on the y-axis between the graphs (C)  
 245 Plot of all knickpoints retreat rates for each experiment. Note the change in scale on the y-axis between  
 246 the graphs. Black dashed line shows the second order polynomial fit to the data used to define the  
 247 normalized longitudinal distance of maximum velocity of knickpoints ( $nDD_{vmax}$ ; see also Fig. S4 in the  
 248 Supplemental Material).

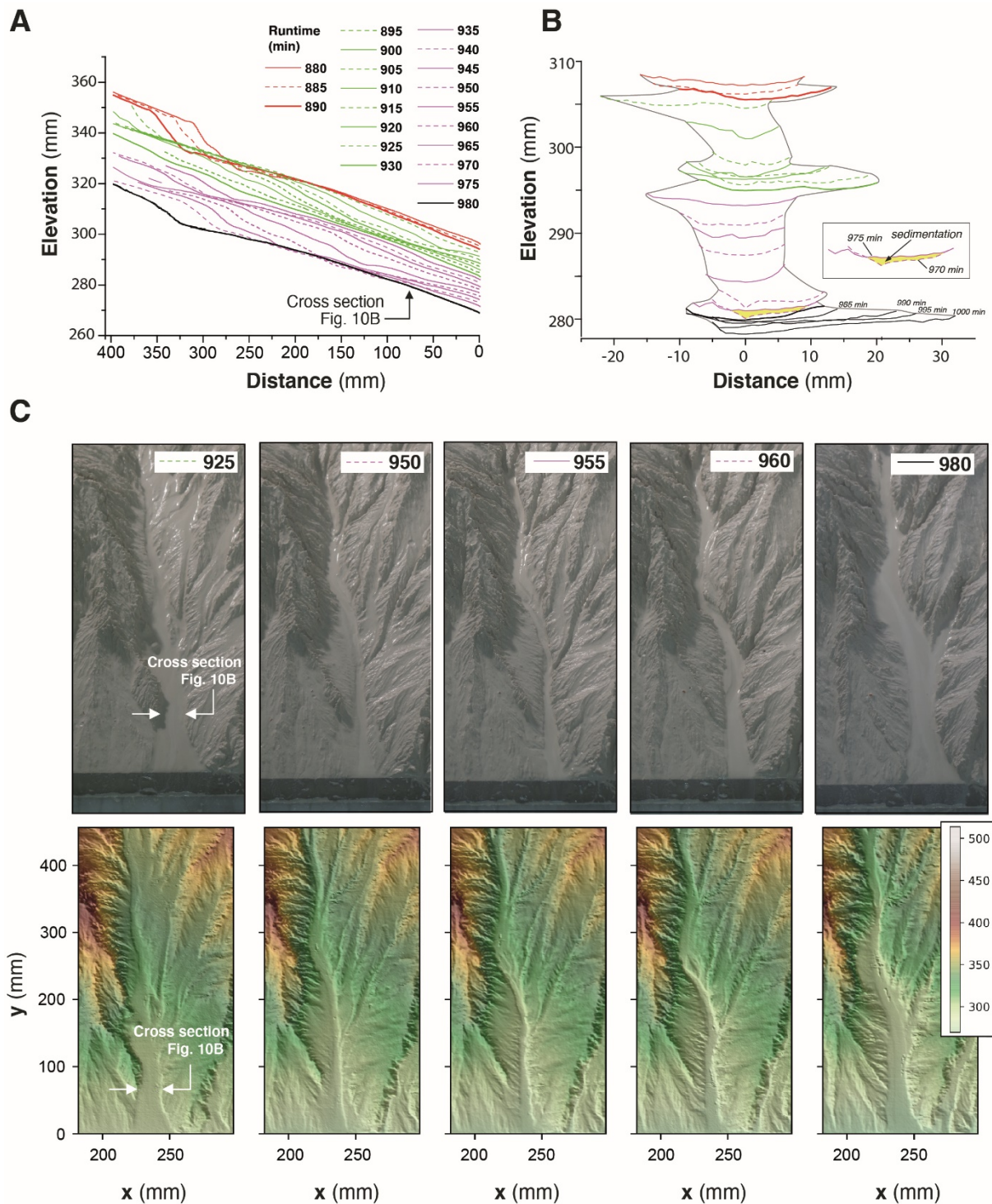


### 249 3.2 Knickpoints initiation

250 To illustrate how knickpoints initiated near the outlet, we consider here a 120 minute-long sequence of  
251 channel evolution in experiment BL15 during which two knickpoints (K1 and K2) successively initiate  
252 and propagate upward (Fig. 10). In addition, we analyzed the history of channel width (Fig. 11A) and  
253 unit water discharge (Fig. 11B) at a cross-section located at 8 cm from the outlet (see location on Fig.  
254 10B). We also present a summary of the statistics of normalized elevation changes (Fig. 11C) and shear  
255 stress (Fig. 11D) for all pixels across the section. The sequence starts with a “standard” profile (i.e., a  
256 typical river profile without any perturbation) at runtimes 880 and 890 min once a previous knickpoint  
257 had already propagated through the section, still visible upstream in Figure 10A. The channel is 23 to  
258 25 mm wide (Fig. 10B and 11A) and the unit discharge is about  $1.5 \cdot 10^6 \text{ mm}^2 \text{ h}^{-1}$ . Erosion in the channel  
259 is on average lower than the base level fall as normalized erosion (erosion rate / base level fall rate) is  
260  $< 1$  for most pixels along the section (Fig. 11C). Then, the knickpoint K1 initiates at runtime 895 min  
261 and starts to propagate upstream. At the surveyed section, the channel first narrows, up to  $\sim 15$  mm wide  
262 at 905 min ( $\sim 60\%$  decrease), and then widens ( $\sim 25$  mm) once the knickpoint has moved upstream of  
263 the section, at 910 min (Fig. 10B). The narrowing phase is naturally associated with an increase of the  
264 unit discharge (Fig. 11B) and with enhanced erosion greater than the base level fall rate, up to 4 times  
265 the base level fall rate in average at 900 min (Fig. 11C), with extremes as high as 8 times the base level  
266 fall rate. Once knickpoint K1 has retreated, unit discharge decreases as the channel subsequently widens,  
267 to reach a width of 25 cm to 28 cm between 925 and 930 min (Fig. 11A) while a new regular profile,  
268 i.e. without any slope break, established at 930 min (Fig. 10A). The normalized erosion across the  
269 section decreases below the base level value (Fig. 11C), with mean erosion rate values of 0.53, 0.36 and  
270 0.76 times below the base level rates between 915 to 925 min. Longitudinally, the profiles stack together  
271 downstream of the knickpoint following its retreat from 895 to 925 min (Fig. 10A), which also indicates  
272 minor vertical erosion here once the knickpoint has retreated despite the ongoing base level falling. The  
273 second knickpoint (K2) then initiates at 935 min, propagates upstream in a similar way, leading to the  
274 setting up of a new regular profile at 980 min downstream its position at that time (Fig. 10A). Channel  
275 narrowing is also observed on the cross-section at the passage of this second knickpoint with a width

276 that decreases to ~15 mm wide (Fig. 10B and 11A), associated with an increase of the unit discharge  
277 and the erosion rate (Fig. 11C). It is followed again by a phase of widening to reach a width to around  
278 30 / 35 mm once the knickpoint has propagated upstream and by a decreasing erosion below the base  
279 level fall rate (Fig. 11C). Again, the longitudinal profiles stack together downstream of the knickpoint  
280 (Fig. 10A). Note that at 975 min, most of the surveyed section is undergoing sedimentation (mean  
281 normalized erosion rate is 0.1 and median is -0.25: Figures 10B and 11C). The distribution of river bed  
282 shear stress along the section is given in the Figure 11D. Despite a large variability along the section,  
283 one can observe a significant increase of the median and maximum values at the time of the knickpoint  
284 passage, both for K1 and K2. Once knickpoints passed, the shear stresses decrease as the river widens.

285 This sequence illustrates that the rivers are never in equilibrium at the 5 min time-scale, but continuously  
286 oscillate over time between disequilibrium states with periods when channel are too wide to keep pace  
287 with the base level, and periods of knickpoint propagation when the erosion is enhanced to catch up the  
288 base level. The river width is the regulation parameter which allows the river erosion to adapt  
289 by increasing or decreasing the unit discharge. These knickpoints then propagate upward up to the divide  
290 as discussed previously (Fig. 6). The average erosion rate is similar to the base level fall rate (mean  
291 normalized erosion rate of the sequence is 0.99) but it does not correspond to any stable configuration  
292 of the river since the erosion rate fluctuates between smaller and larger values. Knickpoints are by-  
293 products of this unsteady dynamics, which are generated during the phases when the river catches up  
294 with its erosion deficit with respect to the base level.

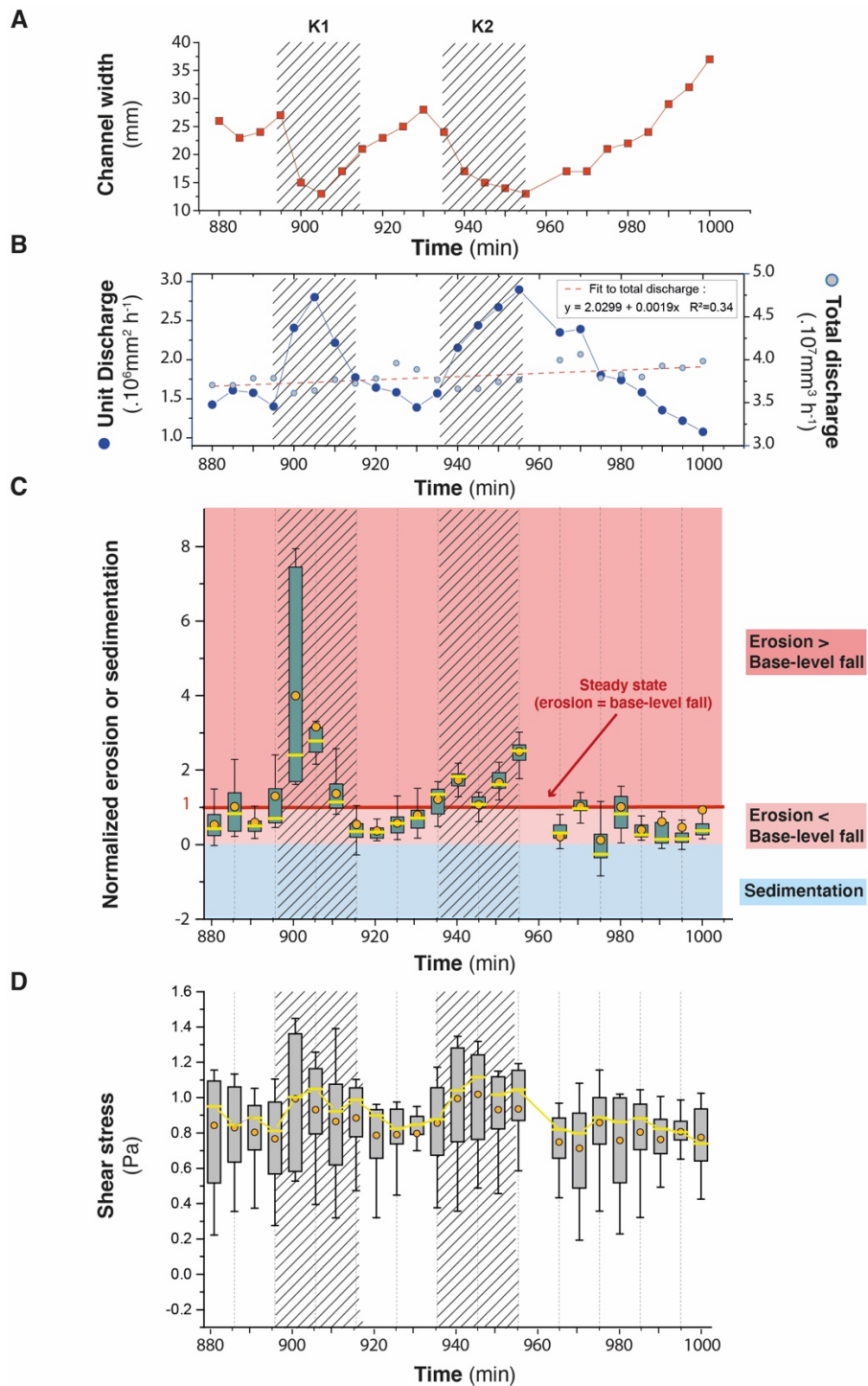


296 **Figure 10.** Downstream knickpoints initiation and propagation in a 120 minute-long sequence of  
 297 experiment BL15 from experimental runtime 880 to 1000 minutes. (A) Sequence of downstream  
 298 longitudinal profiles (5 min time-interval) of the investigated river, corresponding to the sequence  
 299 hydro-geomorphic parameters shown in Figures 11 and 12. Propagation of the first (K1; initiated at  
 300 895') and second (K2; initiated at 935') knickpoints is shown in green and purple colors respectively

301 (see text). (B) Time evolution of successive cross-sections of the channel at 80 mm from the outlet. Colors  
 302 are the same as in Fig. 10A. (C) Photos (top row) and perspective views of DEM (bottom row) at five  
 303 time-steps. Color bar is elevation in mm.

304

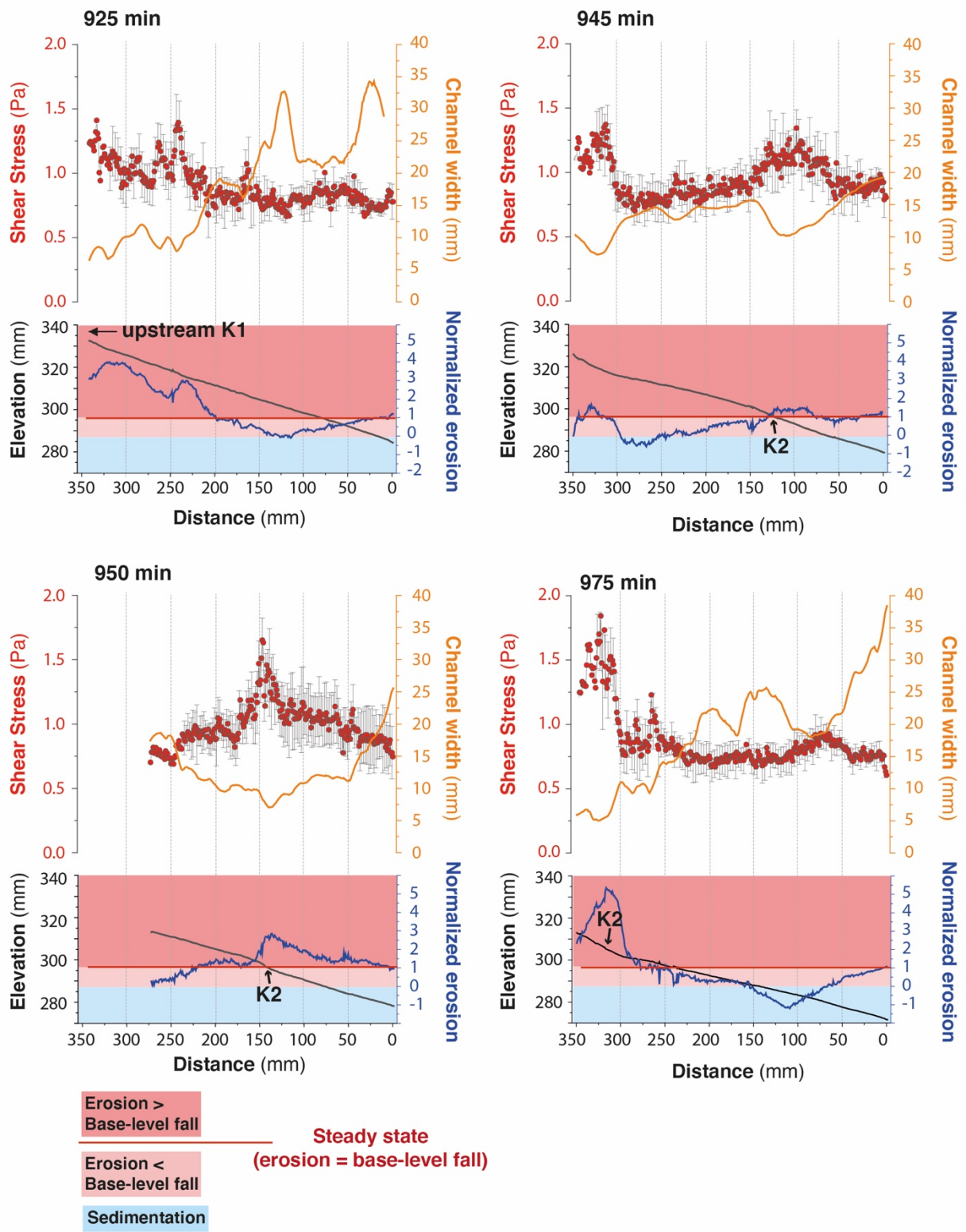
305



306

307 **Figure 11.** Time-series (5 min time interval) of river width (A) and unit and total discharge (B) for the  
308 channel in experiment BL15 shown in Figure 10B (see also location of Fig. 10C). Time-series of box-  
309 and-whisker plots of normalized erosion or sedimentation (C) and shear stress (D) for all pixels across  
310 the channel cross-section. Orange solid circles and yellow lines show the mean and median values,  
311 respectively. Edges of the boxes indicate the 25<sup>th</sup> and 75<sup>th</sup> percentiles. Note that in C, normalized values  
312 of 1 indicate erosion at the same rate as base-level fall (steady-state conditions). Values  $> 1$  or  $< 1$   
313 indicate respectively higher and lower erosion rate than BL fall rate. Negative values indicate  
314 sedimentation. On all graphs, crosshatched areas indicate the passage of knickpoints K1 and K2.

315 To complement cross-section data, we also illustrate (Fig. 12) how parameters vary longitudinally by  
316 considering four stages, two before (925 min) and after (975 min) the passage of the knickpoint K2 and  
317 two during its retreat (945 and 950 min). Note that at 925 min, the previous knickpoint (K1) has just  
318 passed upstream the investigated profile and is responsible for the enhanced normalized erosion and  
319 increased shear stress upstream between distance 200 to 350 mm. Similarly, at 975 min the second  
320 knickpoint (K2) is still in the upstream part of the profile between distance 300 to 350 mm. We also  
321 reported the longitudinal variations in river width, shear stress and normalized erosion along the profiles  
322 (Fig. 12). At runtimes 925 and 975 min, before and after the passage of knickpoint K2, erosion is below  
323 the base level rate along all the profiles down the knickpoints, with even localized sedimentation at 975  
324 min between 50 and ~150 mm. These sections are characterized by low shear stress values, being  
325 between 0.5 and 1 and by rivers that widen downward (around 0.7 mm/cm). On the opposite, during the  
326 passage of knickpoint K2, at runtimes 945 and 950 min, mean shear stress increases locally at the  
327 knickpoint location, being  $> 1$  and the normalized erosion overpasses the base level rate there. These  
328 knickpoint segments are characterized by a narrowing of the rivers as already shown previously. The  
329 data illustrate that erosion mainly occurs during periods of knickpoint retreat though a combination of  
330 local steepening of the profile and narrowing of the river, resulting in an increased shear stress. On the  
331 opposite, once a knickpoint has propagated and between the passage of two successive knickpoints,  
332 erosion decreases significantly and does not longer compensate the base level fall. These periods of  
333 defeated erosion are characterized by low bed shear stress values in wide rivers, that widen downward.



334

335 **Figure 12.** Longitudinal trends of hydro-geomorphic parameters in experiment BL15 at runtimes 925,  
 336 945, 950 and 975 min (see text for comments). K1 and K2: first and second knickpoints discussed in the  
 337 text (see also Fig. 10A).

## 338 **4 Discussion**

### 339 **4.1 Autogenic knickpoints**

340 Our experiments illustrate the generation and retreat of successive knickpoint waves that traveled across  
341 the landscape during the growth of drainage networks. They formed throughout the duration of  
342 experiments independent of the steady precipitation and base level fall rates and of the homogeneity of  
343 the eroded material. These knickpoints were autogenically generated (Hasbargen and Paola, 2000),  
344 arising only from internal geomorphic adjustments within the catchments rather than from variation in  
345 external forcing. Our observations appear very similar to those of Hasbargen and Paola (2000, 2003)  
346 and Bigi et al. (2006) who also reported the generation of successive autogenic knickpoints in landscape  
347 experiments evolving under steady forcing (rainfall and base level fall rate) throughout the duration of  
348 the runs. Unlike our experiments, which mainly consider the growth phase of drainage networks,  
349 experiments reported in Hasbargen and Paola (2000, 2003) and Bigi et al. (2006) considered the  
350 propagation of knickpoints after the phase of network growth, while their system was at steady-state on  
351 average (mean catchment erosion rate equal to base level rate). Then, given that the size of their  
352 experimental catchment was steady over time and given the steady rainfall rate, they were able to rule  
353 out variations of water discharge over time as a main driver for the generation of their knickpoints. On  
354 the opposite, in our experiments the size of catchments continuously increased over time, and thus the  
355 water discharge. However, this does not appear as a key factor controlling knickpoints initiation for  
356 several reasons. First, as we already mentioned, knickpoints arose at all stages of network growth and  
357 divide retreat, for both small and large rivers (Fig. 8), and thus whatever the range of water discharge at  
358 outlet. Second, the migration of the water divide related to drainage network growth occurred steadily  
359 and roughly at a constant rate during the experiments (see Figures 5 and 8), as well as the size of the  
360 catchments and the related increase in water discharge. Thus, we can rule out abrupt variations in  
361 discharge as the driving mechanism for knickpoint initiation. Last, knickpoint initiations occurred at a  
362 higher frequency than the increase in water discharge that resulted from catchment expansion and divide  
363 migration. For example, in addition to unit discharge, we also reported on Figure 11B the variation in  
364 total discharge during the 120 min-long sequence of knickpoint initiation discussed previously. The total

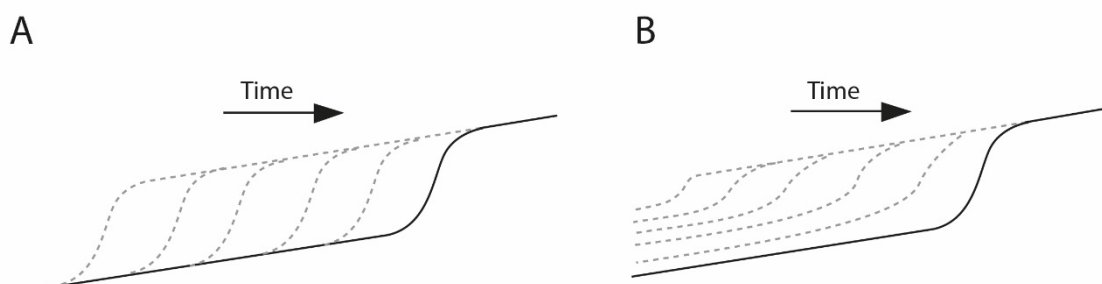
365 discharge rose from  $3.7 \cdot 10^7$  to  $4.0 \cdot 10^7 \text{ mm}^3 \text{ h}^{-1}$  in 120 minutes representing a  $\sim 8\%$  increase, which is  
366 relatively low compared to the  $\sim 100\%$  increase of unit discharge during the passage of a knickpoint.  
367 For all these reasons we conclude that the change in catchment size was not the main driver of successive  
368 knickpoints initiation in our experiments, which occurred at a higher frequency.

#### 369 **4.2 Processes controlling knickpoints initiation and propagation**

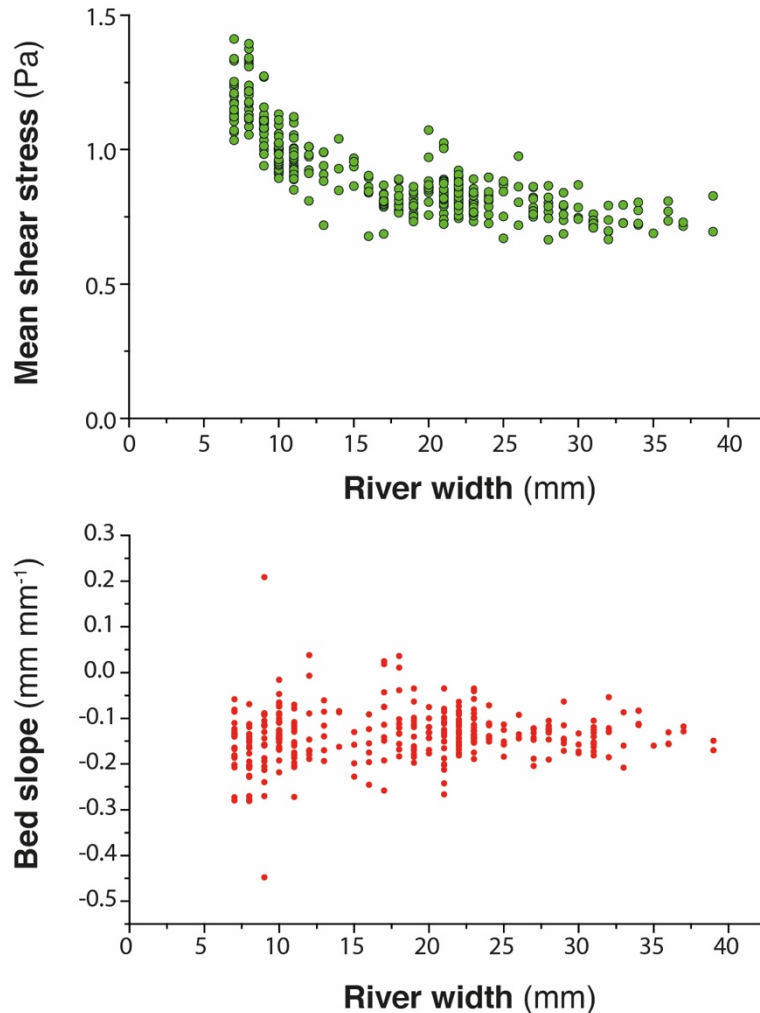
370 Given that the initiation of successive knickpoints was not related to changes in external factors and  
371 catchment size over time, we consider internal geomorphic processes as driving mechanisms. The  
372 detailed sequence of knickpoint initiation and propagation discussed above shows enhanced incision  
373 above the rate of base level fall during the periods of knickpoints propagation. This occurred through  
374 local steepening of the longitudinal profile and narrowing of the river, these two factors lead to an  
375 increase in unit discharge and bed shear stress along the knickpoints. Several studies already  
376 documented how steepening and narrowing act together for increasing river incision rate (e.g. Lavé and  
377 Avouac, 2001; Duvall et al., 2004; Whittaker et al., 2007; Cook et al., 2013), which is what we also  
378 document here. The novelty in our finding here, however, lies in the evolution after knickpoint retreat.  
379 Immediately after the retreat of a knickpoint, we show that erosion in the section of the channel where  
380 the knickpoint just passed is inhibited despite the ongoing base level fall: river incision is lower than the  
381 rate of base level fall, until the passage of a new knickpoint. Although only illustrated in the sequence  
382 detailed previously (Figs. 10 to 12), this was a general behavior that occurred in all three experiments  
383 along their whole longitudinal profile, not only their downstream part as in this sequence. This  
384 systematic decrease in erosion downstream of the knickpoints is inherent to the geometry of the stacks  
385 of all successive longitudinal profiles of each experiment (Fig. 6). In most cases, profiles downstream  
386 of retreating knickpoints stack on top of each other, as illustrated schematically on Figure 13A, which  
387 indicates minor or no erosion downstream of the knickpoints until the passage of a new one. In the case  
388 of continuous steady adjustment of rivers to base level fall downstream of the knickpoints, the geometry  
389 of profiles should instead show a pattern as illustrated in Figure 13B. The pattern of profiles evolution  
390 over time documented here is usually observed following incremental drops in base level (Finnegan,  
391 2013; Grimaud et al., 2016) and to our best knowledge this is the first time here that such geometry is



392 documented in the case of a continuous base level fall. This particular pattern is explained by the  
393 decrease in erosion rate downstream of the retreating knickpoints which acts as if the base level was not  
394 falling continuously at a constant rate but instead dropped regularly step-by-step. Therefore,  
395 understanding the systematic occurrence of successive knickpoints in our experiments requires  
396 understanding why erosion rate dropped downstream of knickpoints, following their retreat. After the  
397 passage of knickpoints, we systematically observe a widening of the rivers, as also documented in  
398 natural systems (e.g. Cook et al., 2014; Zavala-Ortiz et al., 2021) and a decrease in the bed shear stress.  
399 Because an increase in channel width over time inevitably reduces the bed shear stress if discharge and  
400 river gradient remain constant (Fuller et al., 2016), we propose that widening was the main factor  
401 responsible for the decrease in shear stress and erosion rate after the passage of a knickpoint, and thus  
402 for the occurrence of the successive autogenic knickpoints. Demonstrating the sole effect of river width  
403 on bed shear stress and erosion rate is complicated by covariations of these factors with river slope and  
404 variations of discharge related to connection of tributaries. This can be illustrated however on the basis  
405 of the sequence considered previously, particularly at runtime 925 min between the passage of the two  
406 successive knickpoints K1 and K2 (Figs. 10 and 12). At that time, the profile of the river here had a  
407 roughly constant slope (Fig. 14), without any slope break and no major tributary connected (Fig. 10)  
408 that could have significantly changed the water discharge. As illustrated in Figure 12, this river segment  
409 was characterized by widening and decreasing shear stress downward despite constant slope and total  
410 discharge. Thus, this example illustrates a decrease in shear stress that was only the result of the  
411 widening of the river downward (Fig. 14), which supports the hypothesis that decreased erosion  
412 downstream of the propagating knickpoints was mainly due to the widening dynamics of the  
413 experimental rivers.



415 **Figure 13.** Sketches illustrating the difference in the geometry of successive longitudinal profiles  
 416 following the retreat of a knickpoint depending on whether fluvial incision is inhibited (A) or not (B)  
 417 downstream of the retreating knickpoint with respect to the continuously falling base level.



418

419 **Figure 14.** Top: river bed shear stress versus river width in the downstream section, 40 cm-long, of  
 420 experiment BL15 at runtime 925 (see also Fig. 12). Bottom: corresponding slope of the river bed.

421

422 Incision of rivers in our experiments is fundamentally discontinuous despite continuous forcing and we  
 423 highlight downstream river width dynamics, in particular river widening, as a main cause of instability.  
 424 We show that once knickpoints have retreated, unit discharge, shear stress and incision rate all decrease  
 425 downstream while the rivers widen, resulting in a state where incision no longer counterbalances the  
 426 base-level fall. This results in an unstable situation that ends with the initiation and propagation of a new

427 knickpoint and a new sequence of width narrowing, increasing shear stress and incision rate, allowing  
428 the river to recover from the incision delay accumulated during the previous widening period. Further  
429 work is required to understand the mechanisms responsible for lateral channel erosion in our  
430 experiments, which is a key ingredient for understanding river mobility and widening. Several field (e.g.  
431 Hartshorn et al., 2002; Turowski et al., 2008; Fuller et al., 2009), experimental (e.g. Wickert et al., 2013;  
432 Bufe et al., 2016; Fuller et al., 2016; Baynes et al., 2020) and numerical (e.g. Turowski et al., 2007;  
433 Lague, 2010; Langston and Tucker, 2018; Li et al., 2021) studies have demonstrated that high sediment  
434 flux relative to transport capacity promotes increased lateral channel erosion. Most of these studies  
435 highlight the role of cover effect, the protection of the river bed by transient deposition of sediments on  
436 the river bed (Sklar and Dietrich, 2001; Turowski et al., 2007, 2008; Lague, 2010; Baynes et al., 2020;  
437 Li et al., 2021), as a main factor promoting lateral erosion in high sediment flux settings. Other studies  
438 show that by modifying the bed roughness, sediment deposition may deflect the flow, which also  
439 promotes lateral erosion and widening (Finnegan et al., 2007; Fuller et al., 2016). Contrary to  
440 experimental devices specifically designed to address these issues (e.g. Finnegan et al., 2007; Fuller et  
441 al., 2016), direct observation on actual processes that drive lateral erosion in our experiments is made  
442 difficult by the small size of the topographic features, the depth of rivers being of millimeter scale, and  
443 by the low grain size of the material used. Opacity due to the generation of the artificial rainfall also  
444 considerably limits direct observation during the runs. Despite these limitations, data suggest that lateral  
445 erosion and river widening in our experiments is also related to an increase in sediment flux. We show  
446 that knickpoints are locations of enhanced erosion well above the rate of base level fall. We document,  
447 for example, mean erosion rates greater than 5 times the base level fall rate, with extreme values up to  
448 a factor of 8 locally (Fig. 11 and 12). Downstream, where rivers widen, we observe that the general  
449 decrease in erosion rate is also associated with local deposition in some parts of the channels (for  
450 example at runtime 915 min in Figure 11 or 975 min in Figures 10 to 12). We thus hypothesize that  
451 lateral erosion and widening are due in part to the increase sediment flux related to enhanced erosion on  
452 knickpoints. Further work is needed to test this hypothesis, for example by investigating in detail spatio-  
453 temporal variations in erosion and sedimentation during width widening.

454 Further work is also needed to better understand how knickpoints initiate after the phases of widening,  
455 in particular for determining whether river narrowing drives the formation of the knickpoints (e.g. Amos  
456 and Burbank, 2007) or whether narrowing is a consequence of steepening (e.g. Finnegan et al., 2005).  
457 Some studies that investigated river response to increased uplift rate show that narrowing alone, at  
458 constant river gradient, can allow rivers to increase their incision rate (Lavé and Avouac, 2001; Duvall  
459 et al., 2004; Amos et al., 2007). In this context, Amos et al. (2007) propose a model in which the river  
460 response to an increase in uplift rate first involves width narrowing, with the increase in slope and  
461 formation of a knickpoint occurring only in a second stage, if the increase in incision induced by  
462 narrowing is not sufficient to counteract the uplift rate. In our experiments here, we suggest that channel  
463 narrowing predates, and in fact enables, the steepening of the profile in the initial stages of knickpoints  
464 formation. Indeed, we observe that the transition from a wide to a narrow channel occurs very quickly,  
465 at a smaller time scale than the time interval between two successive digitization of the experiments (5  
466 min), and the knickpoints that form then have a very gentle slope, which then amplifies as they migrate  
467 upstream (Fig. 7). This suggests that it is not the steepening that drives river narrowing but on the  
468 contrary that narrowing is essential for knickpoints to initiate. Further work would also be needed to  
469 verify this hypothesis, in particular with additional experiments with much higher frequency of data  
470 acquisition to capture these changes in much more detail.

### 471 **4.3 Implications**

472 Knickpoints in river longitudinal profiles are commonly related to variations in tectonics or climate  
473 through their influence on base level and/or sediment supply (e.g. Whipple and Tucker, 1999; Crosby  
474 and Whipple, 2006; Kirby and Whipple, 2012; Whittaker and Boulton, 2012) and are then used to  
475 highlight such changes when interpreting their occurrence in natural systems. The recognition here that  
476 knickpoints may be generated autogenically due to cycles of river widening and narrowing is then of  
477 first importance for retrieving information on tectonics and climate from their record in landscapes in  
478 the form of knickpoints. Finding criteria that could be used in the analysis of natural systems to  
479 differentiate these autocyclic knickpoints from those formed in response to tectonics or climate would  
480 be an important step in the continuation of this work. A specificity of knickpoints in our experiments is

481 to initiate downstream with a gentle slope, which subsequently steepen in the early stages of migration,  
482 and as a hypothesis we suggest that this may be characteristic of their autogenic formation following the  
483 mechanism described here. Being able to recognize these autogenic knickpoints would also be important  
484 for studies that investigate knickpoints propagation (e.g. Crosby and Whipple 2006; Berlin and  
485 Anderson, 2007; Schwanghart and Scherler, 2020) because knickpoints in our experiments are  
486 characterized by an upward dynamic of retreat that is not conventional. According to stream-power  
487 based celerity models, these studies consider that the upstream propagation rate of knickpoints depends  
488 inversely on drainage area (a proxy for discharge; Crosby and Whipple 2006; Berlin and Anderson,  
489 2007), implying a monotonous decrease of their retreat rate as they propagate upstream due to the  
490 progressive reduction of drainage area and water discharge. This property is used for example to invert  
491 their present location for dating the external perturbation responsible for their formation (Crosby and  
492 Whipple 2006; Berlin and Anderson, 2007). Here, knickpoints in our experiments first accelerate during  
493 their initial stages of propagation before decelerating in a second time as they approach the divide  
494 (Fig.9). Only this later phase of decreasing knickpoint velocity in the upstream part of rivers (for  
495 normalized distance  $NDD > nDD_{V_{max}}$ : Fig. 9) is consistent with predictions from stream-power based  
496 celerity models (see Fig. S5 in the Supplemental Material). On the opposite, a sole control by drainage  
497 area and discharge cannot explain the increase in velocity observed in the downstream sections (for  
498  $NDD < nDD_{V_{max}}$ : Fig. 9), which implies an additional controlling factor. We suggest that this specific  
499 mode of retreat downstream is related to the progressive steepening of the knickpoints rather than to a  
500 purely hydrologic control. Deciphering the respective roles of slope and discharge in the retreat  
501 dynamics documented would require further in-depth analysis, particularly during the early stages of  
502 initiation and propagation which appear to be specific to the autogenic mechanism defined here.

503 We show that the formation of knickpoints in our experiments is closely related to periods of decreasing  
504 erosion rate as the rivers widen, counterbalanced by increasing rate greater than the rate of base level  
505 fall as the rivers narrow and knickpoints form. Thus, the sequential evolution of longitudinal profiles is  
506 very similar to the geometry that would be observed if the system was forced by discrete drops of the  
507 base level, rather than by a continuous drop as it is actually the case. We did not measure the sediment

508 flux at the output of our models, but we can assume that it would be characterized by fluctuations  
509 controlled by the frequency of knickpoint initiation, superimposed on a longer-term increasing trend  
510 related to the growth of drainage networks. Some sediment outflux fluctuations were actually measured  
511 by Hasbargen and Paola (2000) in their experiments and interpreted as the consequence of knickpoint  
512 propagation. This study and our work illustrate that fluctuations in sediment flux can be observed at  
513 catchments outlet despite constant forcing parameters, when autocyclic knickpoints are generated in  
514 river systems.

515 By performing such exploratory experiments, we do not pretend to reproduce natural landscapes in the  
516 laboratory because of important scaling issues (see Paola et al., 2009 for an extensive reflection on this  
517 matter) but rather to highlight and document complex system behaviors under controlled conditions that  
518 could provoke further investigations. Our findings support ongoing investigations that aim in better  
519 understanding the links between lateral erosion, channel geometry and valley width which is an issue  
520 that is emerging in the last years (e.g. Turowski, 2018; Croissant et al., 2019; Langston and Tucker,  
521 2019; Baynes et al., 2020; Zavala-Ortiz et al., 2021). A perspective to our work would be to investigate  
522 the mechanism of knickpoints generation driven by river width variations and the conditions that lead  
523 to their formation using landscape evolution models that incorporate lateral erosion and a dynamic river  
524 width (e.g. Davy et al., 2017; Carretier et al., 2018; Langston and Tucker, 2019). Simulations of  
525 Langston and Tucker (2019) highlight the role of bedrock erodibility as an important factor controlling  
526 lateral migration of rivers and the width of valleys, an issue that has not been investigated here given  
527 the similarity of the eroded materials in our experiments here. This study also confirms the assumption  
528 of Hancock and Anderson (2002) that lateral erosion and widening occurs preferentially in contexts of  
529 low incision rate, *i.e.* in domains with low uplift rate. This is likely in such contexts that the new mode  
530 of autogenic knickpoints formation driven by river width dynamics that we define in this study should  
531 apply.

## 532 **5 Conclusion**

533 Knickpoints in the longitudinal profile of rivers are commonly assumed to be incisional waves that  
534 propagate upstream through landscapes in response to changes in tectonics, climate or base-level. Based

535 on results from a set of laboratory experiments at the drainage basin scale that simulate the growth of  
536 drainage networks in response to constant base level fall and rainfall, we show that knickpoints also  
537 form autogenically, independent of any variations in these external forcing factors. In all experiments,  
538 successive knickpoints initiate and propagate upward throughout the duration of the experimental runs,  
539 independent of the rate of base level fall applied and of the size of the rivers as the catchments expand.  
540 Thanks to the computation of hydraulic information (water depth, river width, discharge and shear  
541 stress) using a hydrodynamic model, we show that the formation of knickpoints is driven by variations  
542 in river width at the outlet of catchments and we highlight width widening as a main cause of instability  
543 leading to knickpoint formation. Widening entails a decrease in shear stress and an incision rate lower  
544 than the rate of base level fall, resulting in an unstable situation that ends up with a sequence of width  
545 narrowing, increasing shear stress and incision rate as a knickpoint initiates. Rivers in our experiments  
546 thus evolve following sequences of width widening and narrowing that drive the initiation and  
547 propagation of successive knickpoints. As a result, incision is fundamentally discontinuous over time  
548 despite continuous forcing. It occurs during discrete events of knickpoint propagation that allow the  
549 rivers to recover from the incision delay accumulated during widening periods.

550

551 **Author contributions.** SB designed the experimental device. LdL, SB and AG built the experimental  
552 setup and carried out the experiments. LdL analyzed the data with the help of SB and PhD. All authors  
553 discussed the data. LdL and SB wrote the manuscript with input from AG and PhD.

554

555 **Acknowledgements.** This work was supported by ORANO-Malvesi and CNRS-INSU Tellus-Syster  
556 programme. We thank Sebastien Carretier and Odin Marc for fruitful discussions and Jens Turowski  
557 for his comments on a preliminary version of this manuscript. We thank Laure Guerit and an  
558 anonymous reviewer for their constructive comments which greatly improved the manuscript.

559

560

561 **References**

- 562 Amos, C.B., and Burbank, D.W.: Channel width response to differential uplift: *J. Geophys. Res.*, 112,  
563 doi:10.1029/2006JF000672, 2007.
- 564 Baynes, E.R.C., Lague, D., Attal, M., Gangloff, A., Kirstein, L.A., and Dugmore, A.J.: River self-  
565 organisation inhibits discharge control on waterfall migration: *Scientific Reports*, v. 8, p. 2444,  
566 doi:10.1038/s41598-018-20767-6, 2018.
- 567 Baynes, E.R.C., Lague, D., Steer, P., Bonnet, S., and Illien, L.: Sediment flux-driven channel  
568 geometry adjustment of bedrock and mixed gravel–bedrock rivers: *Earth Surface Processes and*  
569 *Landforms*, v. 45, p. 3714–3731, doi:10.1002/esp.4996, 2020.
- 570 Berlin, M.M., and Anderson, R.S.: Modeling of knickpoint retreat on the Roan Plateau, western  
571 Colorado: *Journal of Geophysical Research*, v. 112, p. F03S06, doi:10.1029/2006JF000553, 2007.
- 572 Bigi, A., Hasbargen, L.E., Montarani, A., and Paola, C.: Knickpoints and hillslope failure: Interactions  
573 in a steady-state experimental landscape, *in* Willet, C.D., Hovius, N., Brandon, M.T., and Fisher,  
574 D.M., eds. *Tectonics, Climate and Landscape evolution: Geological Society of America Special paper*  
575 *398*, p. 295-307, doi:10.1130/2006.2398(18), 2006.
- 576 Bonnet, S.: Shrinking and splitting of drainage basins in orogenic landscapes from the migration of the  
577 main drainage divide: *Nature Geoscience*, v. 2, p. 766–771, doi:10.1038/ngeo666, 2009.
- 578 Bonnet, S., and Crave, A.: Landscape response to climate change: Insights from experimental  
579 modeling and implications for tectonic versus climatic uplift of topography: *Geology*, v. 31, p. 123–  
580 126, doi: 10.1130/0091–7613, 2003.
- 581 Bufe, A., Paola, C., and Burbank, D.W.: Fluvial beveling of topography controlled by lateral channel  
582 mobility and uplift rate: *Nature geosc.*, 9, 706-710, doi:10.1038/ngeo2773, 2016.
- 583 Cantelli, A., and Muto, T.: Multiple knickpoints in an alluvial river generated by a single drop in base  
584 level: experimental investigation: *Earth Surface Dynamics*, 2, 271-278, doi:10.5194/esurf-2-271-2014,  
585 2014.



586 Carretier, S., Godderis, Y., Maertinez, J., Reich, M., and Martinod, J.: Colluvial deposits as a possible  
587 weathering reservoir in uplifting mountains: *Earth Surf. Dynam.*, 6, 217-237, doi: 10.5194/esurf-6-  
588 217-2018, 2018.

589 Cook, K.L., Turowski, J.M., and Hovius, N.: A demonstration of the importance of bedload transport  
590 for fluvial bedrock erosion and knickpoint propagation: *Earth Surface Processes and Landforms*, v. 38,  
591 p. 683–695, doi:10.1002/esp.3313, 2013.

592 Cook, K.L., Turowski, J.M., and Hovius, N.: River gorge eradication by downstream sweep erosion:  
593 *Nature geoscience*, doi:10.1038/NGEO2224, 2014.

594 Croissant, T., Lague, D., and Davy, P.: Channel widening downstream of valley gorges influenced by  
595 flood frequency and floodplain roughness: *Journal of Geophysical Research-Earth Surface*, v. 124, p.  
596 154–174, doi:10.1029/2018JF004767, 2019.

597 Crosby, B.T., and Whipple, K.X.: Knickpoint initiation and distribution within fluvial networks: 236  
598 waterfalls in the Waipaoa River, North Island, New Zealand: *Geomorphology*, v. 82, p. 16–38,  
599 doi:10.1016/j.geomorph.2005.08.023, 2006.

600 Davy, P., Croissant, T., and Lague, D.: A precipitation method to calculate river hydrodynamics, with  
601 applications to flood prediction, landscape evolution models, and braiding instabilities: *J. Geophys.*  
602 *Res.-Earth*, 122, 1491-1512, doi:10.1002/2016JF004156, 2017.

603 Davy, P., Croissant, T., and Lague, D.: A precipiton method to calculate river hydrodynamics, with  
604 applications to flood prediction, landscape evolution models, and braiding instabilities: *Journal of*  
605 *Geophysical Research-Earth Surface*, v. 122, p. 1491–1512, doi:10.1002/2016JF004156, 2017.

606 Duvall, A., Kirby, E., and Burbank, D.: Tectonic and lithologic controls on bedrock channel profiles  
607 and processes in coastal California: *Journal of Geophysical Research*, v. 109, p. F03002,  
608 doi:10.1029/2003JF000086, 2004.

609 Finnegan, N.J.: Interpretation and downstream correlation of bedrock river terrace treads created by  
610 propagation knickpoints: *Journal of Geophysical Research-Earth Surface*, v. 118,  
611 doi:10.1029/2012JF002534, 2013.

612 Finnegan, N.J., and Dietrich, W.E.: Episodic bedrock strath terrace formation due to meander  
613 migration and cutoff: *Geology*, 39, 143-146, doi:10.1130/G31716.1, 2011.

614 Finnegan, N.J., Roe, G., Montgomery, D.R., and Hallet, B.: Controls on the channel width of rivers:  
615 Implications for modeling fluvial incision of bedrock: *Geology*, 33, 229-232, doi:10.1130/G21171.1,  
616 2005.

617 Fuller, T.K., Perg, L.A., Willenbring, J.K., and Lepper, K.: Field evidence of climate-driven changes  
618 in sediment supply leading to strath terrace formation: *Geology*, 37, 467-470,  
619 doi:10.1130/G25487A.1, 2009.

620 Fuller, T.K., Gran, K.B., Sklar, L.S., and Paola, C.: Lateral erosion in an experimental bedrock  
621 channel: The influence of bed roughness on erosion by bed load impacts: *Journal of Geophysical*  
622 *Research-Earth Surface*, v. 121, p. 1084-1105, doi:10.1002/2015JF003728, 2016.

623 Grimaud, J.-L., Paola, C., and Voller, V.: Experimental migration of knickpoints: influence of style of  
624 base-level fall and bed lithology: *Earth Surface Dynamics*, v. 4, p. 11–23, doi:10.5194/esurf-4-11-  
625 2016, 2016.

626 Hancock, G.S., and Anderson, R.S.: Numerical modeling of fluvial strath-terrace formation in  
627 response to oscillating climate: *Geological Society of America Bulletin*, v. 114, p. 1131-1142, 2002.

628 Hartshorn, K., Hovius, N., Dade, W.B., and Slingerland, R.L.: Climate-driven bedrock incision in an  
629 active mountain belt: *Science*, 297, 2036-2038, 2002.

630 Hasbargen, L.E., and Paola, C.: Landscape instability in an experimental drainage basin: *Geology*, v.  
631 24, p. 1067-1070, 2000.

632 Hasbargen, L.E., and Paola, C.: How predictable is local erosion rate in erosional landscape ? *in*  
633 Wilcox, P.R. and Iverson, R.M., eds., Prediction in Geomorphology: American Geophysical Union  
634 Geophysical Monograph 135, doi:10.1029/135GM16, 2003.

635 Hilley, G.E., and Arrowsmith, J.R.: Geomorphic response to uplift along the Dragon's Back pressure  
636 ridge, Carrizo Plain, California: *Geology*, v. 36, p. 367-370, doi:10.1130/G24517A.1, 2008.

637 Kirby, E., and Whipple, K.X.: Expression of active tectonics in erosional landscapes: *Journal of*  
638 *Structural Geology*, v. 44, p. 54–75, doi:10.1016/j.jsg.2012.07.009, 2012.

639 Lague, D.: Reduction of long-term bedrock incision efficiency by short-term alluvial cover  
640 intermittency: *J. Geophys. Res.*, 115, doi:10.1029/2008JF001210, 2010.

641 Lague, D., Crave, A., and Davy, P.: Laboratory experiments simulating the geomorphic response to  
642 tectonic uplift: *Journal of Geophysical Research-Solid Earth*, v. 108, doi:10.1029/2002JB001785,  
643 2003.

644 Langston, A.L., and Tucker, G.E.: Developing and exploring a theory for the lateral erosion of  
645 bedrock channels for use in landscape evolution models: *Earth Surf. Dynam.*, 6, 1-27,  
646 doi:10.5194/esurf-6-1-2018, 2018.

647 Lavé, J., and Avouac, J.P.: Fluvial incision and tectonic uplift across the Himalayas of central Nepal:  
648 *Journal of Geophysical Research-Solid Earth*, v. 106, p. 26561–26591, doi:10.1029/2001JB000359,  
649 2001.

650 Li, T., Venditti, J.G., and Sklar, L.S.: An analytical model for lateral erosion from saltating bedload  
651 particle impacts: *J. Geophys. Res.– Earth*, 126, doi:10.1029/2020JF006061, 2021.

652 Mitchell, N.A., and Yanites, B.J.: Spatially variable increase in rock uplift in the Northern U.S.  
653 Cordillera recorded in the distribution of river knickpoint and incision depths: *Journal of Geophysical*  
654 *Research: Earth Surface*, v. 124, 1238-1260, doi:10.1029/2018JF004880, 2019.

655 Moussirou, B., and Bonnet, S.: Modulation of the erosion rate of an uplifting landscape by long-term  
656 climate change: An experimental investigation: *Geomorphology*, v. 303, p. 456–466,  
657 doi:10.1016/j.geomorph.2017.12.010, 2018.

658 Paola, C., Straub, K., Mohrig, D., and Reinhardt, L.: The “unreasonable effectiveness” of stratigraphic  
659 and geomorphic experiments: *Earth-Science Reviews*, v. 97, p. 1–43,  
660 doi:10.1016/j.earscirev.2009.05.003, 2009.

661 Rohais, S., Bonnet, S., and Eschard, R.: Sedimentary record of tectonic and climatic erosional  
662 perturbations in an experimental coupled catchment-fan system: *Basin Research*, v. 24, p. 198–212,  
663 doi:10.1111/j.1365-2117.2011.00520.x, 2012.

664 Scheingross, J.S., Lamb, M.P., and Fuller, B.M.: Self-formed bedrock waterfalls: *Nature*, v. 567, p.  
665 229–233, doi:10.1038/s41586-019-0991-z, 2019.

666 Schwanghart, W.S., and Scherler, D.: Divide mobility controls knickpoint migration on the Roan  
667 Plateau (Colorado, USA): *Geology*, 48, 698-702, doi:10.1130/G47054.1, 2020.

668 Singh, A., Reinhardt, L., and Fofoula-Georgiou, E.: Landscape reorganization under changing  
669 climatic forcing: Results from an experimental landscape: *Water Resources Research*, v. 51, p. 4320–  
670 4337, doi:10.1002/2015WR017161, 2015.

671 Sklar, L.S., and Dietrich, W.E.: Sediment and rock strength controls on river incision into bedrock:  
672 *Geology*, 29, 1087-1090, 2001.

673 Sweeney, K.E., Roering, J.J., and Ellis, C.: Experimental evidence for hillslope control of landscape  
674 scale: *Science*, v. 349, p. 51–53, doi:10.1126/science.aab0017, 2015.

675 Tofelde, S., Savi, S., Wickert, A. D., Buße, A., and Schildgen, T. F.: Alluvial channel response to  
676 environmental perturbations: fill-terrace formation and sediment-signal disruption. *Earth Surface*  
677 *Dynamics*, v. 7, p. 609-631, doi:10.5194/esurf-7-609-2019, 2019.

678 Turowski, J.M.: Alluvial cover controlling the width, slope and sinuosity of bedrock channels: *Earth*  
679 *Surface Dynamics*, v. 6, p. 29–48, doi:10.5194/esurf-6-29-2018, 2018.

680 Turowski, J.M., Lague, D., Crave, A., and Hovius, N.: Experimental channel response to tectonic  
681 uplift: *Journal of Geophysical Research-Earth Surface*, v. 111, doi:10.1029/2005JF000306, 2006.

682 Turowski, J.M., Lague, D., and Hovius, N.: Cover effect in bedrock abrasion: A new derivation and its  
683 implication for the modeling of bedrock channel morphology: *J. Geophys. Res.*, 112,  
684 doi:10.1029/2006JF000697, 2007.

685 Turowski, J.M., Hovius, N., Meng-Long, H., Lague, D., and Men-Chiang, C.: Distribution of erosion  
686 across bedrock channels: *Earth Surf. Process. Landforms*, 33, 353-363, doi:10.1002/esp.1559, 2008.

687 Whipple, K.X., and Tucker, G.E.: Dynamics of the stream-power river incision model: Im- plications  
688 for height limits of mountain ranges, landscape response timescales, and research needs: *Journal of*  
689 *Geophysical Research*, v. 104, p. 17,661–17,674, 1999.

690 Whittaker, A.C., and Boulton, S.J.: Tectonic and climatic controls on knickpoint retreat rates and  
691 landscape response times: *Journal of Geophysical Research*, v. 117, F02024, doi:10  
692 .1029/2011JF002157, 2012.

693 Whittaker, A.C., Cowie, P.A., Attal, M., Tucker, G.E., and Roberts, G.P.: Bedrock channel adjustment  
694 to tectonic forcing: Implications for predicting river incision rates: *Geology*, v. 35, p. 103,  
695 doi:10.1130/G23106A.1, 2007.

696 Wickert, A.D., Martin, J.M., Tal, M., Kim, W., Sheets, B., and Paola, C.: River channel lateral  
697 mobility: Metrics, time scales, and controls: *J. Geophys. Res.-Earth*, 118, 396-412,  
698 doi:10.1029/2012JF002386, 2013.

699 Zavala-Ortiz, V., Carretier, S., Regard, V., Bonnet, S., Riquelme, R., and Choy, S.: Along-stream  
700 variations in valley flank erosion rates measured using  $^{10}\text{Be}$  concentrations in colluvial deposits from  
701 canyons in the Atacama Desert: *Geophysical Research Letters*, 48, doi:10.1029/2020GL089961, 2021.